

Deployable cuboctahedrons for adaptive space infrastructure

Stephanie J. Woodman¹, Alex Moore¹, Siona Tagare¹, Kenneth Cheung² and Rebecca Kramer-Bottiglio¹

Abstract—Diverse space infrastructure is required for exploration missions to the Moon, Mars, and beyond. However, the cost of sending materials into space is high. One approach to ease this cost is the use of adaptive infrastructure, which may leverage discrete building blocks that can be assembled, disassembled, and reassembled into diverse mechanical structures based on the relevant environment and task demands. Indeed, the NASA Automated Reconfigurable Mission Adaptive System (ARMADAS) project is taking this approach. The discrete building component selected by ARMADAS engineers is a cuboctahedron, or more simply a “voxel,” as a volumetric pixel. The voxels are lightweight and simple, and assemble into programmable mechanical metamaterial structures with high stiffness and stability. However, transportation of complete voxels remains volume-inefficient, and fabrication of voxels in-situ adds notable complexity to the system. Herein, we introduce a cuboctahedron voxel design that compresses to 35% of its deployed volume during transport and passively locks in its expanded state at its destination, where a multitude of voxels can then be assembled. Inspired by the Hoberman sphere, the voxel is designed to deploy using a 1D force input. We further confirm that the new deployable voxel is compatible with existing ARMADAS assembly agents.

Index Terms—shape-changing robots, morphing robots, modular infrastructure, reconfigurable infrastructure

I. INTRODUCTION

Modular, lightweight, and reconfigurable infrastructure that can be easily assembled, disassembled, and reassembled could apply to diverse sectors such as humanitarian aid, disaster relief, and space exploration. For example, areas impacted by storms, fires, or flooding require quick deployment of infrastructure such as wireless antennas for restoring communication, scaffolding for restoring power, or tents for impromptu patient care. Off-planet, NASA is interested in the capability to build infrastructure such as solar power, communications, railway, and habitat systems in space or on extraterrestrial bodies. Key requirements include ease of transportation (low volume and mass during transport to the destination), adaptability (global reconfiguration), and structural stability (an ability to withstand infrastructure-level loads).

S.J.W. was supported by a NASA NSTGRO Fellowship (80NSSC22K1188). R.K.B. was supported by NASA grant 80NSSC20M0098. A.M. was supported by the National Science Foundation (NSF) under IIS-1954591. S.T. was supported by the NSF under EFMA-1830870. K.C. was supported by the NASA STMD Game Changing Development Program (ARMADAS Project).

¹Department of Mechanical Engineering and Materials Science, Yale University, New Haven, CT, USA stephanie.woodman@yale.edu

²Intelligent Systems Division, NASA Ames Research Center, Moffett Field, CA, USA kenny@nasa.gov

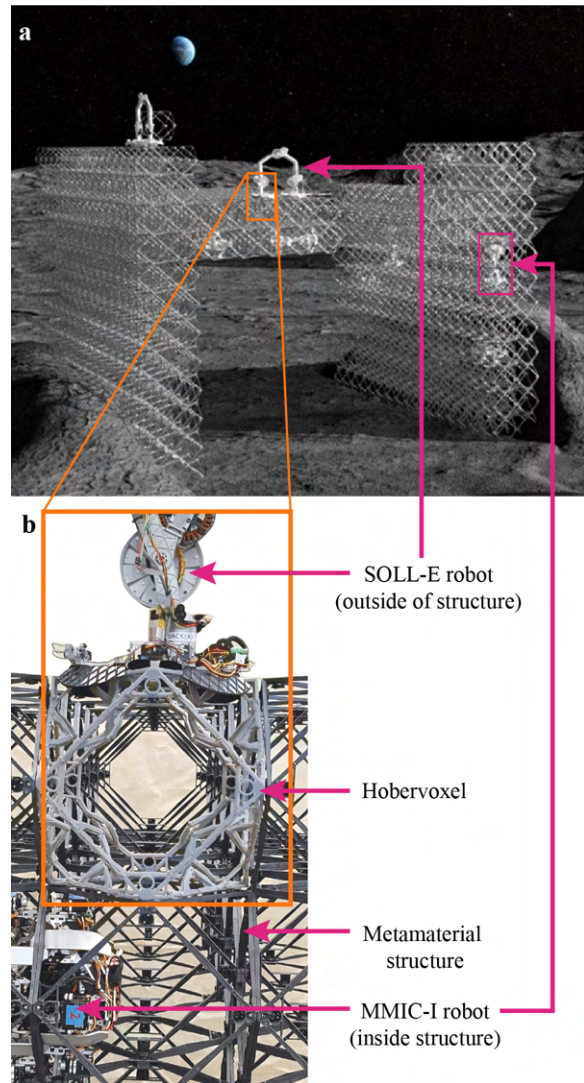


Fig. 1. ARMADAS platform for adaptable space infrastructure. **a.** Vision of the system assembling infrastructures in an extraterrestrial environment. **b.** Our deployable Hobervoxel integrated into the present system, surrounded by static voxels and with assembly agent robots.

Inspired by the collective works on reconfigurable and shape-changing robots [1]–[4] as well as high-performance mechanical metamaterials [5]–[7], NASA’s Coded Structures Laboratory (CSL) at the NASA Ames Research Center has been developing the Automated Reconfigurable Mission Adaptive Digital Assembly Systems (ARMADAS) [8] project to extend the re-usability and material efficiency of modular

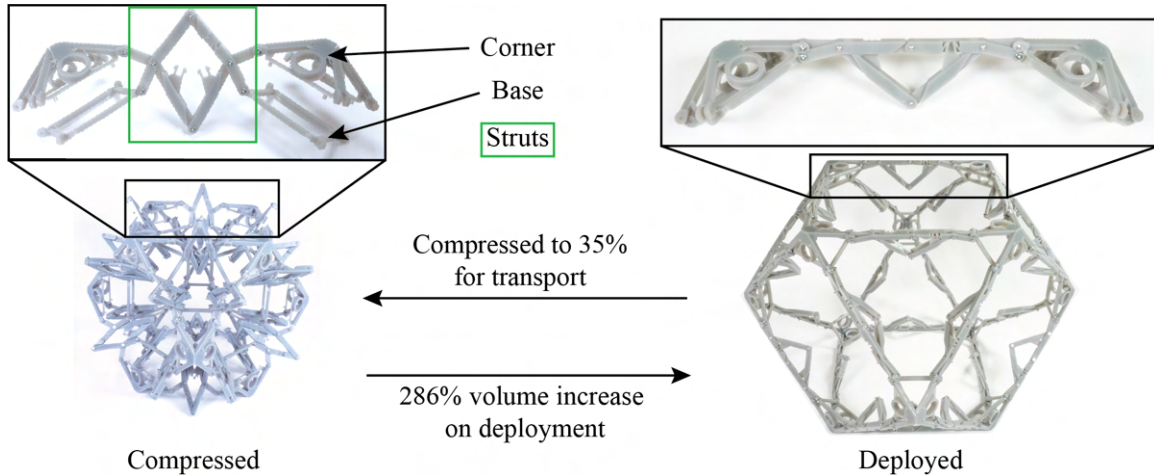


Fig. 2. **Design overview and expansion ratio.** Both the contracted and expanded versions of the Hobervoxel, with key features identified.

engineered systems to space infrastructure that is robotically assembled and maintained (Fig. 1a-b). The ARMADAS team has designed static and ultralight modules, called “voxels,” which are made of a carbon fiber composite [9] that outlines a cuboctahedron shape. The voxels can be assembled together into cuboctahedral lattice materials, then disassembled and reassembled into variable large-scale structures based on the environment or use demands [8], [10]. The ARMADAS team has further developed two robots, both on the same scale as the voxels, which autonomously complete the assembly tasks. One type of robot carries and places voxels (“SOLL-E” [11], Fig. 1b), while another moves within the structure to secure voxels together (“MMIC-I” [12], [13], Fig. 1b). Overall, the ARMADAS system is reliable due to the simplicity of the task-specific robots, and the ultralight voxels render the assembled structures extremely mass efficient [14], [15].

Though the ARMADAS system is light, strong, and adaptable, the voxels take up a large fixed volume and thus are very costly to transport. Therefore, we introduce an augmented voxel design that can be initially collapsed and then deployed when needed. We aim to create voxels that take up a lower storage volume during transport, and then irreversibly expand into the original voxel building block once in the target environment. Inspired by the global contraction/expansion of a Hoberman sphere based on a single degree of freedom (DoF) input, we applied Hoberman linkages to the cuboctahedron voxels. The Hoberman sphere achieves its contraction and expansion due to its rings of scissor pairs, each composed of two struts, connected at pivot points [16]. Analyses have explored the Hoberman sphere’s kinematics [17], symmetry [18], and generality [19]. In simulation and a close-to-ideal case, the Hoberman sphere can contract to just 12.5% of its initial volume [20]. The Hoberman mechanism has previously been applied to several robots, including a snake-inspired swallowing robot using sequential Hoberman rings [21], a soft jet propulsion system that rapidly compresses to expel water and generate thrust [20], and a

shape-adaptive mobile robot [22]. However, the advantages of a Hoberman-type approach have not been investigated in weight- and space-limited scenarios where the Hoberman design would need to perform similarly to a static, non-deployable system once expanded.

We applied the Hoberman mechanism to the ARMADAS voxels to create a deployable voxel, which we call a Hobervoxel. The Hobervoxel compresses to 35% of its initial volume (inversely, increasing in volume by 286% between the contracted and expanded states) and passively locks into a rigid cuboctahedron when expanded. The expanded cuboctahedron further matches the geometry of the static voxels and is compatible with the locking [23] and gripping [13] mechanisms on the ARMADAS assembly robots. Our Hobervoxels provide a pathway to programmable, adaptive space infrastructure by adding a layer of volumetric shape change to the system.

II. DESIGN AND FABRICATION

Our Hobervoxel design was determined by 1) the ARMADAS system’s operational constraints (e.g., voxel assembly and attachment mechanisms), 2) 1 DoF force input for deployment, and 3) the need for structural strength, rivaling that of the static voxel in the expanded form (Fig 2).

A. Operational constraints

The current assembly agent robots developed by NASA’s ARMADAS project create two design constraints. First, the SOLL-E robot, which carries and places voxels as it crawls over the lattice structures, is tailored to the specific cuboctahedron voxel geometry (Fig. 3a), with 203 mm edge lengths, in order to grip and traverse the voxels. Second, the MMIC-I robot, which fastens voxels together using an androgynous fastening mechanism [23], requires a particular geometry of the voxel corners (Fig. 3b). This geometry has circular holes to hold the fasteners and gripping bars for both robots, resulting in a rigid pyramid structure at each corner. Our Hobervoxel design retains the specific shape,

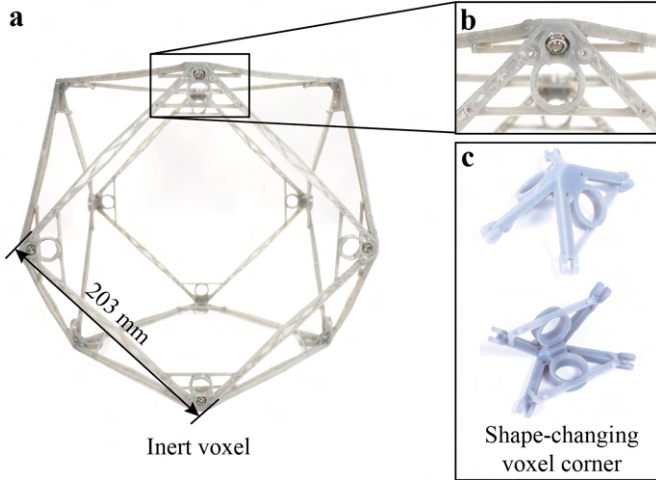


Fig. 3. **Static voxel form factor.** **a.** The complete static voxel with a characteristic length of the system. **b.** The corner of the static voxel with robot and fastener interface features. **c.** The corner of the Hobervoxel is made to replicate the corner of the static voxel.

dimensions, and vertex geometry as the original static voxels to maintain compatibility with the assembly agents (Fig. 3c).

B. Hobervoxel deployment

Working within the operational constraints, we aim to reduce the volume of the voxel for transport using a simple compression mechanism.

Our approach is inspired by the compression and expansion of the Hoberman sphere, which actuates using a single, uniaxial force input. Each vertex in a Hoberman sphere has an internal and external component, which are the “base” and “corner,” respectively, in our design (Fig. 2). The vertices are joined by a scissor mechanism, comprising two pairs of two struts, Strut 1 and Strut 2 (Fig. 4a,b), where Strut 1 connects to the base, and Strut 2 connects to the corner (Fig. 2). Holistically, the Hoberman sphere works by preserving the relative geometry and orientation of the vertices during compression. Using our terminology, this means that the corners and bases follow fixed relative trajectories, as dictated by the geometry of the scissor mechanism. The corner and base pieces move axially away from the center of the cuboctahedron during expansion while maintaining their orientation relative to the other vertices.

We developed a simulation to find and optimize a scissor linkage geometry that would meet the above constraints for motion. The simulation is based on a closed-form geometric model that uses a strut length of 60 mm (Fig. 4a,b) and a Strut 1 height of 5.5 mm (Fig. 4a) based on the operational constraints detailed in § II.A. The equations comprising this model are detailed in § VI for completeness. The free variables of the model are length L and angle ϕ of Struts 1 and 2 (Fig. 4a,b). These variables characterize the width and height of the isosceles triangle formed when the scissor mechanism expands (Fig. 4c).

In a scissor mechanism that produces the desired trajectories, the orange and pink points in Fig. 4c must closely follow the blue and purple ideal trajectories (shown in Fig. 4c,d), respectively. The blue line refers to the axial trajectory of the corner and base, while the horizontal purple line refers to the constant orientation of the vertices. To characterize the performance of a mechanism with specific L and ϕ , we calculated the optimal position of the orange and pink points at each increment of folding in the simulated scissor mechanism. Specifically, we ensured that, at each increment of folding, the tracked points were as close as they could be to the ideal trajectory. We recorded these positions and used them to plot the mechanism’s optimal simulated trajectory, as in Fig. 4d.

To find functional and spatially efficient solutions, we swept L and ϕ values and calculated a quality metric for each pair in order to compare their performance. We took the distance between the ideal and calculated trajectories at every point along the lines and set the quality metric as the standard deviation of these distances, which could be expressed as

$$\sigma(A) \quad \text{for } A = \{T^{calc}_y(a) - T^{ideal}_y(a) \mid a=1:240\}$$

where $T^{calc}_y(a)$ is the y-coordinate of the calculated trajectory at increment a along the trajectory, $T^{ideal}_y(a)$ is the y-coordinate of the ideal trajectory at increment a along the trajectory, and the trajectory is divided into 240 increments.

We then plotted the quality metric over the space of all possible mechanisms defined by L and ϕ , where smaller values of the quality metric described mechanisms whose calculated trajectory was closer to the ideal path (Fig. 4e). The simulated results did not account for the fact that some solutions are physically impossible, like values of L approaching 60 mm. Thus, the chosen design was not simply the mechanism with the smallest quality metric, especially because many different $\{L, \phi\}$ pairs have a sufficiently small quality metric, but are non-functional in practice. Ultimately, the chosen design, shown as the red star in Fig. 4e, set $L = 40$ mm and $\phi = 40^\circ$. This was a middle-ground between a minimized quality metric and maximized mechanical feasibility. This design achieved a compression ratio of 35% (Fig. 2), the theoretical ideal given the large size of our corners.

C. Hobervoxel structural strength

After designing the deployment mechanism, we sought to make the Hobervoxel robust enough to act as a permanent structural component once deployed. We printed all parts on a Formlabs Form 3+ resin printer, due to the need for precision at small scales, and assembled the parts with 0-80 hardware. Without any locking mechanisms, the Hobervoxel tends to contract toward its low-volume state. To solve this problem, we chose to use two locking mechanisms based on rivets and buckles.

To lock the base and corner pieces together, we integrated split-shank rivets (Fig. 5b) onto the corners and corresponding receiving holes into the bases. As the Hobervoxel deploys, the rivets move toward their receiving holes and

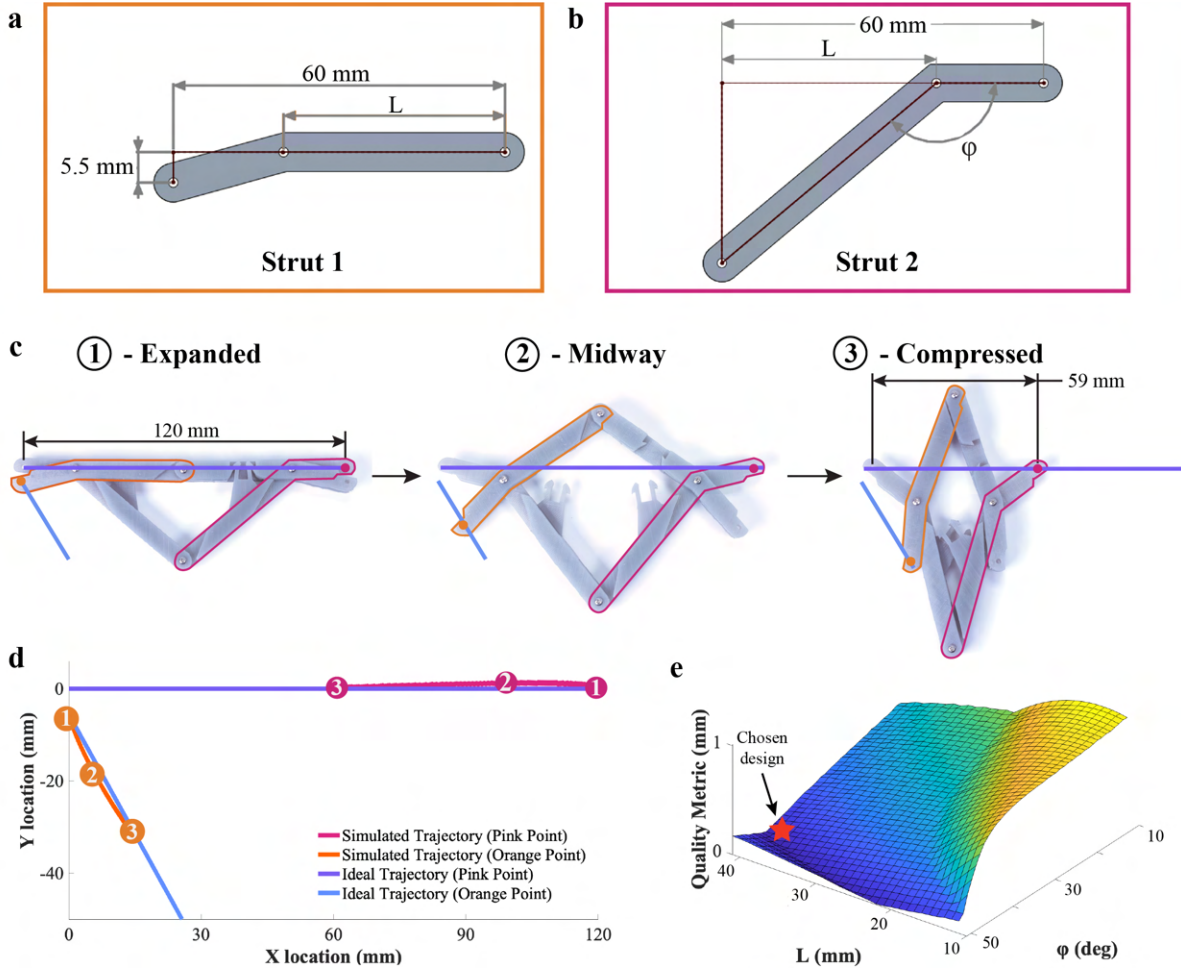


Fig. 4. **Identifying an optimal design using simulation.** **a.** Strut 1 of a 2-strut scissor pair with constraints called out, and the variable L that was optimized in the simulation. **b.** Strut 2 of a 2-strut scissor pair with constraints called out, and the variables L and ϕ that were optimized in the simulation. **c.** Two scissor pairs that make up an edge of the compressible voxel showing three points along the trajectory of (d), and the expanded and compressed edge lengths. Strut 1 highlighted in orange, Strut 2 highlighted in pink, and the ideal trajectories in purple and blue. **d.** The calculated trajectory results of the simulated L, ϕ pair and how they compare to the ideal trajectories. **e.** Varied L and ϕ plotted against their quality metric, with the chosen design pointed out.

permanently lock each base and corner together once it is completely deployed.

The scissor mechanisms undergo a higher combined load than the bases and corners and thus require a more robust mechanism to rigidly lock them once deployed. We integrated buckles to provide locking and rigidity. The bottom two struts have the male portion of the buckle, and the top two struts have the female part. The male part locks into the female part as the Hobervoxel deploys (Fig. 5a). Once expanded, the scissor mechanism is impossible to fold further because its yoke-style design would cause parts of the struts to interfere, and cannot be unfolded without the large force required to snap the prongs in the male buckle. The buckles act as stabilizing tension elements between the top and bottom struts when the scissor mechanisms are locked, increasing their rigidity. Importantly, the Hobervoxel's uniform volumetric expansion means both the buckle and rivet mechanisms lock passively, as all mating pieces simultaneously move toward

each other. The locking mechanism requires a strong and elastic material that allows the male buckles and rivet heads to flex temporarily before snapping into the expanded position, which led us to choose Formlabs' Tough 1500 resin for our Hobervoxel prototypes.

III. EXPERIMENTAL DESIGN

After designing the Hobervoxel, we aimed to quantify the differences in mechanical performance between the static and deployable voxels, so we fabricated them out of the same resin. Since these voxels will ultimately make up a cuboctahedral lattice metamaterial and be treated as a cellular solid, we additionally compare the performance of the voxel subunits to their constituent material—Tough 1500 resin—as a baseline to evaluate the geometric designs.

To capture the differences in mechanical performance, we tested a cylinder of the neat Tough 1500 resin (5 samples), the static voxel fabricated with the same resin (3 samples),

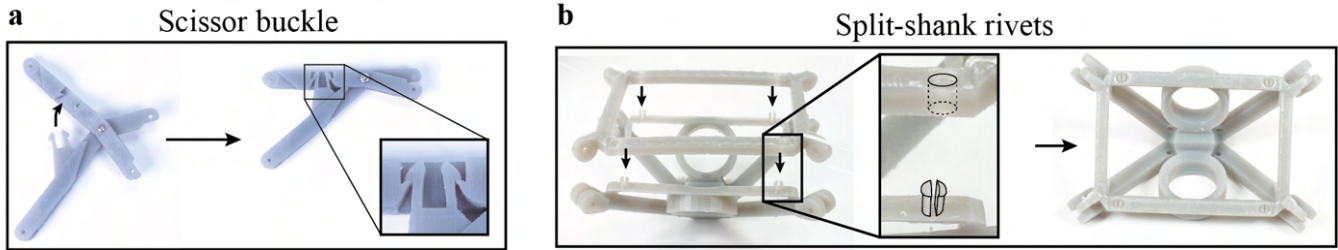


Fig. 5. **System rigidity and locking.** **a.** The buckle that locks the scissor pairs together in the expanded state. **b.** The split-shank rivets that lock the corner to the base.

and the Hobervoxel again fabricated with the same resin (3 samples), in compression according to ASTM D695-15 (Fig. 6). From this data, we extracted the average compressive strength of each sample and used this, along with the average weights of the samples, to get the strength-to-weight ratios (σ WRs) (Table I). We also calculated the stiffness as the slope of the linear regions, the elastic modulus, and the proportional limit (stress just before plastic deformation at the end of the elastic region).

IV. RESULTS

The Hobervoxel has a higher compressive strength and strength-to-weight ratio (σ wR) than the static voxel (Fig. 6b,c, Table I). An interesting property of the Hobervoxel is that we did not see the traditional decrease in stress with increasing strain beyond the ultimate tensile strength point during the compression testing. Before our Hobervoxel samples could fail traditionally, the internal corners of the structure hit each other, causing the stress to increase dramatically at the highest strain. We expected to see a decreasing stress-strain relation much sooner due to added joints in the Hobervoxel relative to the static voxel. Instead, the Hobervoxel showed many stick-slip points that let the stress increase slowly, but continuously, even to extreme strains. Given this, we took our compressive strength as the maximum strength before the structure contacted itself.

The neat material showed the highest compressive strength, σ WR, stiffness, elastic modulus, and proportional limit—orders of magnitude above both voxel types. Though the neat material is impressive, it would weigh too much at larger scales to be worth the increases in strength—the structure would be overbuilt with solid blocks. The Hobervoxels had higher average stiffness, elastic modulus, and proportional limit than the static voxels, though they were on the same order of magnitude, showing an overall increase in mechanical performance than the static voxels.

V. DISCUSSION

The Hobervoxel saw an increase in mechanical performance compared to the static voxel, with benefits in σ WR, stiffness, elastic modulus, and proportional limit, while significantly improving volumetric efficiency for space transport. The results indicate that the Hoberman mechanism is a feasible approach to creating a deployable cuboctahedron

voxel. As we saw failure modes only within the struts on both voxel types, we estimate that the increased performance metrics of the Hobervoxels are due to the increased bulk of the struts.

This study was constructed using the same material for both the static and deployable voxel prototypes, such that the differences in mechanical performance would generalize across other materials for future systems. Indeed, because the Hobervoxel includes additional hinges, locking mechanisms, and strut bulk relative to the static voxel, we expect the slight performance increases to generalize due to increased weight, with the assumed reduction in volume during travel (allowing for fewer trips with material) outweighing the weight penalty. Nevertheless, given the ARMADAS static voxel geometry used here is optimized for weight and mechanical performance when manufactured from a carbon fiber-reinforced polymer material, it will be necessary to carry out the same static vs. deployable voxel comparisons with the specialized material in the future.

Aside from material choice and design refinement, an important next step will be to implement an actuation mechanism for deployment from the compressed state once in the target environment. A few methods have been discussed, including the development of a new assembly agent robot that would move voxel to voxel with a simple inflating or linear actuator, expanding the voxels into their locked forms. Another approach may be a spring-loaded design that could be transported in a constrained volume, and then automatically expand when released from the constraint.

In general, robotic assembly of structural modules is seen as a strong candidate solution for very large space structures, such as habitats, antennas, industrial facilities, and scientific instrumentation requiring large apertures. While there are ongoing efforts to develop the ability to source material from space, near-term operations will rely heavily on materials launched from Earth, at an extremely high cost. Therefore, these structures must be highly efficient—in the low-gravity environments currently considered, this naturally favors frameworks of modules that are composed of slender struts, like the voxels presented herein. An ability to pack and deploy such structural modules onsite presents an appealing alternative to the robotic or manual assembly of modules from stock strut and node parts. Thus, the Hobervoxel and

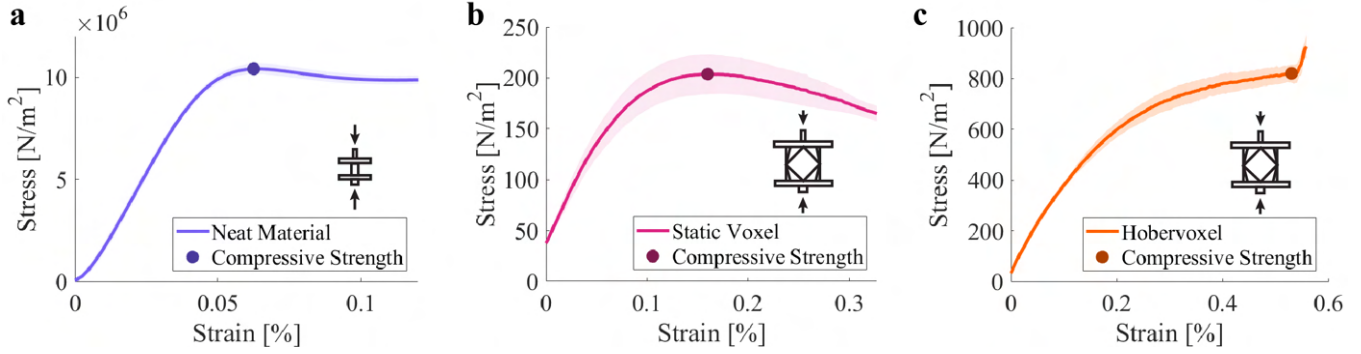


Fig. 6. **Results of compression testing.** Stress vs. strain for the **a** neat material, **b** static voxel, and **c** Hobervoxel, with the compressive strength identified. Error clouds represent one standard deviation.

Sample	Mass [g]	σ WR [$N/kg * m^2$]	Stiffness [N/m]	Elastic Modulus [N/m^2]	Proportional Limit [N/m^2]
Neat Material	3.73	2.79e3	4.38e6	2.71e8	7.27e6
Static Voxel	211.9	9.61e-4	654.3	3.87e3	106.5
Hobervoxel	491.2	16.70e-4	2.16e3	7.15e3	125.1

TABLE I
MECHANICAL PERFORMANCE METRICS OF NEAT MATERIAL, STATIC VOXEL, AND HOBERVOXEL.

ARMADAS system may be understood as a conceptual bridge between a status quo of manually assembled space systems and an envisioned future of deployable and robotically assembled space systems. Such hybrid deployed and assembled systems hold promise in realizing the benefits of both types of systems where appropriate.

We hope that this Hoberman-inspired voxel deployment strategy will be broadly used to achieve large volumetric shape-change across the fields of modular and soft robotics and adaptive infrastructure. In the context of this project, our simulation and design approach show promise for use in NASA's ARMADAS system, the deployment of which will enable the next phase of space exploration to the Moon, Mars, and beyond.

VI. EQUATIONS FOR THE GEOMETRIC MODEL

This set of equations describes the geometry and motion of the scissor linkage mechanism during compression, which we used to simulate the system. L , and ϕ (Fig. 4a,b) describe the geometry of the scissor mechanism: L is the length of the portion of the scissor closer to the center, and ϕ is the angle of the bend in Strut 2. In our chosen case, $L = 40$ mm and $\phi = 40^\circ$. D is a constant describing the length of each strut, which was 60 mm.

The variables ρ and δ control the position of the mechanism in simulation, where ρ dictates how folded the scissor is, and δ dictates its overall angle relative to the coordinate axes. Simulating over small increments of ρ and δ ensures smoothness in the simulation results (Fig. 4d,e). The calculated values ψ_1 and ψ_2 refer to the location of the labeled pink and orange points, respectively, from Fig. 4c. For example,

ψ_{x_1} is the X coordinate of the pink point. The set of equations that describe the system are:

$$d = \frac{5.5}{\sin\left(\tan^{-1}\left(\frac{5.5}{D-L}\right)\right)}$$

$$\theta = \tan^{-1}\left(\frac{5.5}{D-L}\right)$$

$$b = \frac{L}{\cos(\phi)}$$

$$\kappa = \left((D-L)^2 + b^2 - 2(D-L) * b * \cos(\pi - \phi)\right)^{\frac{1}{2}}$$

$$\eta = \sin^{-1}\left(\frac{b * \sin(\pi - \phi)}{\kappa}\right)$$

$$\gamma = \phi - \eta$$

$$h = \left(L^2 + b^2 - 2 * b * l * \cos(\pi - \rho + \phi)\right)^{\frac{1}{2}}$$

$$\alpha = 2\sin^{-1} = \left(\frac{L * \sin(\pi - \rho + \phi)}{h}\right)$$

$$\epsilon = (2\kappa^2 - 2\kappa^2 \cos(\alpha + 2\gamma))^{\frac{1}{2}}$$

$$\sigma = \left((D-L)^2 + d^2 - 2d(D-L)\cos(\pi - \rho + \theta)\right)^{\frac{1}{2}}$$

$$N = \sin^{-1}\left(\frac{d\sin(\pi - \rho + \theta)}{\sigma}\right)$$

$$\psi_{x_1} = \epsilon * \cos\left(\frac{\pi - \alpha - 2\gamma}{2} + \delta - \eta\right)$$

$$\psi_{y_1} = \epsilon * \sin\left(\frac{\pi - \alpha - 2\gamma}{2} + \delta - \eta\right)$$

$$\psi_{x_2} = \sigma \sin(\delta - N)$$

$$\psi_{y_2} = \sigma \cos(\delta - N)$$

REFERENCES

- [1] D. Shah, B. Yang, S. Kriegman, M. Levin, J. Bongard, and R. Kramer-Bottiglio, "Shape changing robots: bioinspiration, simulation, and physical realization," *Advanced Materials*, vol. 33, no. 19, p. 2002882, 2021.
- [2] M. Yim, W.-m. Shen, B. Salemi, D. Rus, M. Moll, H. Lipson, E. Klavins, and G. S. Chirikjian, "Modular self-reconfigurable robot systems [grand challenges of robotics]," *IEEE Robotics Automation Magazine*, vol. 14, no. 1, pp. 43–52, 2007.
- [3] K. H. Petersen, N. Napp, R. Stuart-Smith, D. Rus, and M. Kovac, "A review of collective robotic construction," *Science Robotics*, vol. 4, no. 28, p. eaau8479, 2019.
- [4] P. Thalamy, B. Piranda, and J. Bourgeois, "A survey of autonomous self-reconfiguration methods for robot-based programmable matter," *Robotics and Autonomous Systems*, vol. 120, oct 2019.
- [5] T. A. Schaedler, A. J. Jacobsen, and W. B. Carter, "Toward lighter, stiffer materials," *Science*, vol. 341, no. 6151, pp. 1181–1182, 2013.
- [6] K. Bertoldi, V. Vitelli, J. Christensen, and M. Van Hecke, "Flexible mechanical metamaterials," *Nature Reviews Materials* 2017 2:11, vol. 2, pp. 1–11, oct 2017.
- [7] J. U. Surjadi, L. Gao, H. Du, X. Li, X. Xiong, N. X. Fang, and Y. Lu, "Mechanical Metamaterials and Their Engineering Applications," *Advanced Engineering Materials*, vol. 21, p. 1800864, mar 2019.
- [8] C. E. Gregg, D. Catanoso, O. I. B. Formoso, I. Kostitsyna, M. E. Ochalek, T. J. Olatunde, I. W. Park, F. M. Sebastianelli, E. M. Taylor, G. T. Trinh, and K. C. Cheung, "Ultralight, strong, and self-reprogrammable mechanical metamaterials," *Science robotics*, vol. 9, p. eadi2746, jan 2024.
- [9] K. C. Cheung and N. Gershenfeld, "Reversibly assembled cellular composite materials," *Science*, vol. 341, no. 6151, pp. 1219–1221, 2013.
- [10] B. Jenett, A. Abdel-Rahman, K. Cheung, and N. Gershenfeld, "Material-Robot System for Assembly of Discrete Cellular Structures," *IEEE Robotics and Automation Letters*, vol. 4, pp. 4019–4026, jul 2019.
- [11] I. W. Park, D. Catanoso, O. Formoso, C. Gregg, M. Ochalek, T. Olatunde, F. Sebastianelli, P. Spino, E. Taylor, G. Trinh, and K. Cheung, "SOLL-E: A Module Transport and Placement Robot for Autonomous Assembly of Discrete Lattice Structures," in *IEEE International Conference on Intelligent Robots and Systems*, (Detroit, MI), 2023.
- [12] E. Niehs, A. Schmidt, C. Scheffer, D. E. Biediger, M. Yannuzzi, B. Jenett, A. Abdel-Rahman, K. C. Cheung, A. T. Becker, and S. P. Fekete, "Recognition and Reconfiguration of Lattice-Based Cellular Structures by Simple Robots," *Proceedings - IEEE International Conference on Robotics and Automation*, pp. 8252–8259, may 2020.
- [13] O. Formoso, G. Trinh, D. Catanoso, I. W. Park, C. Gregg, and K. Cheung, "MMIC-I: A Robotic Platform for Assembly Integration and Internal Locomotion through Mechanical Meta-Material Structures," *Proceedings - IEEE International Conference on Robotics and Automation*, vol. 2023-May, pp. 7303–7309, 2023.
- [14] N. B. Cramer, D. W. Cellucci, O. B. Formoso, C. E. Gregg, B. E. Jenett, J. H. Kim, M. Lendraitis, S. S. Swei, G. T. Trinh, K. V. Trinh, and K. C. Cheung, "Elastic shape morphing of ultralight structures by programmable assembly," *Smart Materials and Structures*, vol. 28, apr 2019.
- [15] C. E. Gregg, J. H. Kim, and K. C. Cheung, "Ultra-light and scalable composite lattice materials," *Advanced Engineering Materials*, vol. 20, no. 9, p. 1800213, 2018.
- [16] C. Hoberman, "Reversibly expandable doubly-curved truss structure," oct 1988.
- [17] J. Cai, Y. Xu, and J. Feng, "Kinematic analysis of Hoberman's Linkages with the screw theory," *Mechanism and Machine Theory*, vol. 63, pp. 28–34, may 2013.
- [18] Y. Chen, L. Fan, and J. Feng, "Kinematic of symmetric deployable scissor-hinge structures with integral mechanism mode," *Computers Structures*, vol. 191, pp. 140–152, oct 2017.
- [19] Z. You and S. Pellegrino, "Foldable bar structures," *International Journal of Solids and Structures*, vol. 34, pp. 1825–1847, may 1997.
- [20] S. Iacoponi, G. Picardi, M. Chellapurath, M. Calisti, and L. Cecilia, "Underwater soft jet propulsion based on a hoberman mechanism," *2018 IEEE International Conference on Soft Robotics, RoboSoft 2018*, pp. 449–454, jul 2018.
- [21] Y. Zhang, Z. Qian, H. Huang, X. Yang, and B. Li, "A Snake-Inspired Swallowing Robot Based on Hoberman's Linkages," *Journal of Mechanisms and Robotics*, vol. 14, dec 2022.
- [22] D. E. Geyer and C. J. Turner, "A Spatial Linkage Exoskeleton for a Shape-Adaptive Mobile Robot," *Proceedings of the ASME Design Engineering Technical Conference*, vol. 1, nov 2019.
- [23] O. Formoso, C. Gregg, G. Trinh, A. Rogg, and K. Cheung, "Androgynous Fasteners for Robotic Structural Assembly," *IEEE Aerospace Conference Proceedings*, mar 2020.